



# CHALMERS

## Chalmers Publication Library

### **On the analysis of the dc dynamics of multi-terminal VSC-HVDC systems using small signal modeling**

This document has been downloaded from Chalmers Publication Library (CPL). It is the author's version of a work that was accepted for publication in:

**IEEE PowerTech Conference 2013**

Citation for the published paper:

Pinares, G. ; Tjernberg, L. ; Le, T. (2013) "On the analysis of the dc dynamics of multi-terminal VSC-HVDC systems using small signal modeling". IEEE PowerTech Conference 2013

Downloaded from: <http://publications.lib.chalmers.se/publication/186170>

Notice: Changes introduced as a result of publishing processes such as copy-editing and formatting may not be reflected in this document. For a definitive version of this work, please refer to the published source. Please note that access to the published version might require a subscription.

Chalmers Publication Library (CPL) offers the possibility of retrieving research publications produced at Chalmers University of Technology. It covers all types of publications: articles, dissertations, licentiate theses, masters theses, conference papers, reports etc. Since 2006 it is the official tool for Chalmers official publication statistics. To ensure that Chalmers research results are disseminated as widely as possible, an Open Access Policy has been adopted. The CPL service is administrated and maintained by Chalmers Library.

(article starts on next page)

# On the analysis of the dc dynamics of multi-terminal VSC-HVDC systems using small signal modeling

Gustavo Pinares

Lina Bertling Tjernberg

Le Anh Tuan

Department Energy and Environment  
Division of Electric Power Engineering  
Chalmers University of Technology  
412 96 Gothenburg, Sweden  
gustavo.pinares@chalmers.se

Claes Breitholtz

Department Signals and Systems  
Division of Automatic Control  
Chalmers University of Technology  
412 96 Gothenburg, Sweden

Abdel-Aty Edris

Quanta Technology  
Oakland, CA, 94612 USA

**Abstract**— In this paper, an analysis of the dc dynamics of multi-terminal VSC-HVDC systems using the small signal modeling method is presented. Usually, the VSC controllers are designed under the consideration that they operate independently of each other. However, the possible interactions among them and the dc grid should be studied, especially in multi-terminal topologies. In this paper, three VSC-HVDC systems are modeled and, after linearization, the eigenvalues of the system are calculated for different loading conditions. The results from this analysis are compared to those obtained from more detailed models using PSCAD. It is shown that the operating point, the gains of the direct-voltage controller and the cable dynamics have an impact on the system performance.

**Index Terms**—Multi-terminal VSC-HVDC system, small signal analysis, eigenvalues, control systems, dc dynamics.

## I. INTRODUCTION

In recent years, multi-terminal voltage-source-converter-based HVDC systems (VSC-MTDC) have been proposed as an option for the interconnection of renewable energy resources, and for the integration of electricity markets over large geographical areas [1]. Voltage source converters (VSC) have been found to be a promising technology, mainly due to their specific controllability features. Moreover, with the development of multilevel converters, the losses level has been reduced considerably and the voltage waveform generated by the VSC has been improved dramatically [2]. However, the VSC technology has still some limitations to overcome, such as the development of reliable protection schemes and the development of control strategies.

The topic of control strategies deals with the selection of the control modes of the converters connected to the dc grid. For example, in [3] it was shown the importance of the direct-voltage, which can be used as an indicator of power balancing in the dc system. Likewise, in [4] and [5] it was shown the advantage of the voltage margin and the voltage droop control for balancing the power flow in the dc side of VSC-MTDC during contingencies. Some manufacturers also propose the

use of the voltage droop control along with a “secondary control” signal which determines the final power set-point to the converters [6].

Frequently, the dynamic evaluation of the proposed control strategies for MTDC systems, such as the ones presented in [4]-[5], are based on extensive electromagnetic transient simulations, while approaches based on analytical methods have been used to less extent. Examples of the use of analytical methods in the topic of control of VSC-MTDC can be seen in [7]-[9], where the small signal analysis is used. For instance, a stability evaluation of two control strategies for the inner current controller is performed in [7] using the small signal analysis. The eigenvalues of a five-terminal system are calculated for different short circuit ratios and it was found that the use of the direct-voltage as a feedback control signal improves the performance of the system. Furthermore, in [8], the choice of the slope for the voltage-droop characteristic was addressed by a frequency response criterion. The idea is that the multivariable gain of the system should not exceed a certain threshold for any selected slope. In [9], a more systematic approach to develop a small signal model of a VSC-MTDC system was presented. The system was divided into subsystems to be finally merged into the final VSC-MTDC system model. The dynamics of the system was evaluated for different controller gains. The ranges in which the gains make the system eigenvalues located in the stable region of the complex plane (s-plane) were determined.

The control system of the upcoming VSC-MTDC will bring a number of challenges. In such systems, the simultaneous operation of complex elements such as converters and dc cables can result in undesired behavior. Therefore, there is a need for developing analytical tools for evaluating the dynamical performance of VSC-MTDC systems. The small signal method is used in this paper, focusing the analysis on the dc dynamics. Some reports disregard the analysis of the dc dynamics by assuming the dc network being composed only by resistances [4], [5], [9]. However, in this paper, the capacitance and inductances from

the grid are not neglected. Furthermore, the previous cited reports analyzed the VSC-MTDC with its entire complexity implying dealing with several problems simultaneously. In case problems are found, this may make difficult to identify the source behind. In this paper, however, some assumptions are made in order to limit the scope of the problem to only the dc side of the system.

The organization of the paper is as follow: In Section II, the system is linearized around an operating point and a procedure to find the state space (SS) model of the system is presented. In Section III, the SS model is used to find the eigenvalues of the system for the recommended system parameters and controller gains. Since the system is nonlinear, the dependency of the eigenvalues on the operating point is shown as well. The results are finally compared with a more detailed model using PSCAD simulations. In Section VI, final remarks on the findings of the performed studies are presented.

## II. SYSTEM MODELING

### A. Assumptions

In order to focus the analysis only on the dc dynamics, the following assumptions are made:

- The AC sources are represented as infinite buses, i.e., the voltage and phase angle of the voltage  $V_s$  are constants.
- The elements are considered ideal, i.e., the high frequency harmonics generated by the switching action of power electronic valves are ignored. Capacitors, inductors, and resistors are linear, temperature and frequency independent.
- The measuring devices are ideal. The signals coming from these devices are instantaneous with no distortion.

The models are proposed with these assumptions. The conclusions from the analysis will be, therefore, only due to the interaction between converter controllers and the dc grid.

### B. State Space Model of the converter

The typical control structure of a VSC is illustrated in Figure 1. The core of the control system is the current controller which is implemented using the vector control method. With this method, the alternating three-phase quantities (voltages and currents) are transformed into two-component dc quantities, the so called  $dq$  frame. In order to perform the transformation, the rotating speed  $\omega_s$  and the angle  $\theta_s$  are calculated by the phase-locked loop (PLL) block. Open loop model

The open-loop model of the VSC can be described by the following set of equations in the  $dq$  frame [9], [10]:

$$\frac{di_{sd}}{dt} = -\frac{R}{L}i_{sd} + \omega_s i_{sq} + \frac{1}{L}V_s - \frac{1}{L}V_{cd} \quad (1a)$$

$$\frac{di_{sq}}{dt} = -\frac{R}{L}i_{sq} - \omega_s i_{sd} - \frac{1}{L}V_{cq} \quad (1b)$$

$$i_{DC} = \frac{V_{cd}i_{sd} + V_{cq}i_{sq}}{E_{DC}} \quad (1c)$$

where  $R$  is the resistance and  $L$  is the inductance of the phase reactor,  $i_{sd}$  and  $i_{sq}$  are the  $d$  and  $q$  component of the current  $i_s$ , respectively,  $V_{cd}$  and  $V_{cq}$ , are the  $d$  and  $q$  component of the voltage  $V_c$ , respectively, and  $\omega_s$  is the ac grid frequency.

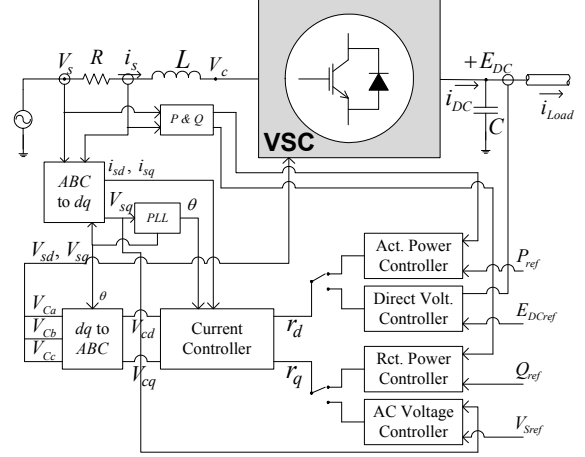


Figure 1. Typical VSC control structure.

It should be noted that the VSC capacitor dynamic equation is not considered in the above set of equations. The capacitor dynamic is considered as part of the dc grid dynamics.

The states are  $i_{sd}$  and  $i_{sq}$ , the inputs are  $V_{cd}$  and  $V_{cq}$ , and the output is  $i_{DC}$ . It is important to realize that in (1c) there are products of an input multiplied by a state, making the system nonlinear. The nonlinearities are linearized around an operating point, resulting in the following small signal model:

$$\dot{\Delta \mathbf{i}}_{sdq} = \mathbf{A}_s \Delta \mathbf{i}_{sdq} + \mathbf{B}_s \Delta \mathbf{V}_{cdq} \quad (2a)$$

$$\Delta i_{DC} = \mathbf{C}_s \Delta \mathbf{i}_{sdq} + [\mathbf{D}_{s1} \quad \mathbf{D}_{s2}] \begin{bmatrix} \Delta \mathbf{V}_{cdq} \\ \Delta E_{DC} \end{bmatrix} \quad (2b)$$

where:

$$\Delta \mathbf{i}_{sdq}^T = [\Delta i_{sd} \quad \Delta i_{sq}] \quad \Delta \mathbf{V}_{cdq}^T = [\Delta V_{cd} \quad \Delta V_{cq}]$$

$$\mathbf{A}_s = \begin{bmatrix} -\frac{R}{L} & \omega_s \\ -\omega_s & -\frac{R}{L} \end{bmatrix} \quad \mathbf{B}_s = \begin{bmatrix} -\frac{1}{L} & 0 \\ 0 & -\frac{1}{L} \end{bmatrix} \quad \mathbf{C}_s = \begin{bmatrix} \frac{V_{cd0}}{E_{DC0}} & \frac{V_{cq0}}{E_{DC0}} \end{bmatrix}$$

$$\mathbf{D}_{s1} = \begin{bmatrix} \frac{i_{sd0}}{E_{DC0}} & \frac{i_{sq0}}{E_{DC0}} \end{bmatrix} \quad \mathbf{D}_{s2} = \begin{bmatrix} -\frac{P_{DC0}}{E_{DC0}^2} \end{bmatrix} \quad P_{DC0} = V_{cd0}i_{sd0} + V_{cq0}i_{sq0}$$

Note that, since the ac system is assumed to be infinite, the PLL dynamics can be disregarded, and  $\Delta V_s$  becomes zero.

#### 1) AC current controller

The structure of current controller is shown in Figure 2. The current controller is composed of a proportional-integral controller with a cross coupling compensation and a feed forward term of the voltage  $V_s$  (however,  $\Delta V_s = 0$ ). If the modulation indices are normalized with respect to the voltage  $E_{DC}$  [12] and considering the assumption that measuring

devices are ideal, the following equations, in terms of small perturbation, are obtained for the current controller:

$$\Delta V_{cd} = -k_{pcc}(\Delta r_d - \Delta i_{sd}) - k_{icc} \int_0^t (\Delta r_d - \Delta i_{sd}) dt + \omega_s L \times \Delta i_{sd} \quad (3)$$

$$\Delta V_{cq} = -k_{pcc}(\Delta r_q - \Delta i_{sq}) - k_{icc} \int_0^t (\Delta r_q - \Delta i_{sq}) dt - \omega_s L \times \Delta i_{sq} \quad (4)$$

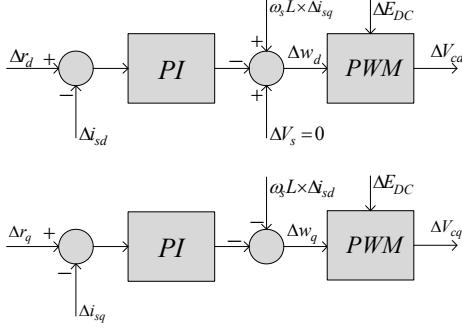


Figure 2. Current controller.

This can be expressed in an SS form as:

$$\dot{\mathbf{m}}_{dq} = -\mathbf{B}_{cc} \Delta \mathbf{i}_{sdq} + \mathbf{B}_{cc} \Delta \mathbf{r}_{dq} \quad (5a)$$

$$\Delta \mathbf{V}_{cdq} = -\mathbf{C}_{cc} \mathbf{m}_{dq} + \mathbf{D}_{cc1} \Delta \mathbf{i}_{sdq} - \mathbf{D}_{cc2} \Delta \mathbf{r}_{dq} \quad (5b)$$

where:

$$\mathbf{m}_{dq}^T = [m_d \quad m_q] \quad \Delta \mathbf{r}_{dq}^T = [\Delta r_d \quad \Delta r_q]$$

$$m_d = k_{icc} \int_0^t (\Delta r_d - \Delta i_{sd}) dt \quad m_q = k_{icc} \int_0^t (\Delta r_q - \Delta i_{sq}) dt$$

$$\mathbf{B}_{cc} = \begin{bmatrix} k_{icc} & 0 \\ 0 & k_{icc} \end{bmatrix} \quad \mathbf{C}_{cc} = \mathbf{I}_{2 \times 2}$$

$$\mathbf{D}_{cc1} = \begin{bmatrix} k_{pcc} & \omega_s L \\ -\omega_s L & k_{pcc} \end{bmatrix} \quad \mathbf{D}_{cc2} = \begin{bmatrix} k_{pcc} & 0 \\ 0 & k_{pcc} \end{bmatrix}$$

Equation (2) combined with (5) leads to the SS model of a converter together with its current controller, as follows:

$$\Delta \dot{\mathbf{x}} = \mathbf{A}_c \Delta \mathbf{x} + [\mathbf{B}_{c1} \quad \mathbf{B}_{c2}] \begin{bmatrix} \Delta \mathbf{r}_{dq}^T \\ \Delta E_{DC} \end{bmatrix} \quad (6a)$$

$$\Delta i_{DC} = \mathbf{C}_c \Delta \mathbf{x} + [\mathbf{D}_{c1} \quad \mathbf{D}_{c2}] \begin{bmatrix} \Delta \mathbf{r}_{dq}^T \\ \Delta E_{DC} \end{bmatrix} \quad (6b)$$

where:

$$\Delta \mathbf{x}^T = [\Delta i_{sdq}^T \quad \mathbf{m}_{dq}^T \quad n] \quad \mathbf{A}_c = \begin{bmatrix} \mathbf{A}_s + \mathbf{B}_s \mathbf{D}_{cc1} & -\mathbf{B}_s \mathbf{C}_{cc} \\ -\mathbf{B}_{cc} & \mathbf{0}_{2 \times 2} \end{bmatrix} \quad \mathbf{B}_{c1} = \begin{bmatrix} -\mathbf{B}_s \mathbf{D}_{cc2} \\ \mathbf{B}_{cc} \end{bmatrix}$$

$$\mathbf{B}_{c2} = \mathbf{0}_{4 \times 1} \quad \mathbf{C}_c = [\mathbf{C}_s + \mathbf{D}_{s1} \mathbf{D}_{cc1} \quad -\mathbf{D}_{s1} \mathbf{C}_{cc}] \quad \mathbf{D}_{c1} = -\mathbf{D}_{s1} \mathbf{D}_{cc2} \quad \mathbf{D}_{c2} = \mathbf{D}_{s2}$$

## 2) Direct-voltage controller

The output of the direct-voltage controller is connected to the input  $\Delta r_d$  of the current controller (see Figure 1). This is illustrated in Figure 3 where the direct-voltage controller is connected to the model of the converter described by (6). The direct-voltage controller is a proportional-integral controller, which can be described by the following equation:

$$\Delta r_d = k_{pEdc} (\Delta r_{Edc} - \Delta E_{DC}) + k_{iEdc} \int_0^t (\Delta r_{Edc} - \Delta E_{DC}) dt \quad (7)$$

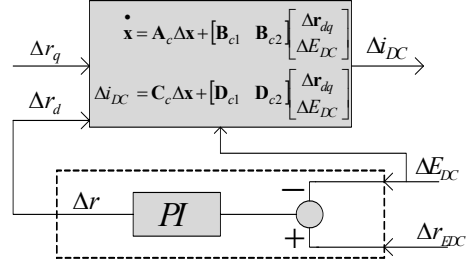


Figure 3. Direct-voltage controller.

Considering also the input  $\Delta r_q$ , the direct-voltage controller can be expressed in an SS form as:

$$\dot{\mathbf{n}} = \mathbf{B}_{Edc1} \Delta \mathbf{r}_{edq} - \mathbf{B}_{Edc2} \Delta E_{DC} \quad (8a)$$

$$\Delta \mathbf{r}_{dq} = \mathbf{C}_{Edc} \mathbf{n} + \mathbf{D}_{Edc1} \Delta \mathbf{r}_{edq} - \mathbf{D}_{Edc2} \Delta E_{DC} \quad (8b)$$

where:

$$\Delta \mathbf{r}_{edq}^T = [\Delta r_{Edc} \quad \Delta r_q] \quad n = k_{iEdc} \int_0^t (\Delta r_{Edc} - \Delta E_{DC}) dt$$

$$\mathbf{B}_{Edc1} = [k_{iEdc} \quad 0] \quad \mathbf{B}_{Edc2} = k_{iEdc} \quad \mathbf{C}_{Edc} = \begin{bmatrix} 1 \\ 0 \end{bmatrix}$$

$$\mathbf{D}_{Edc1} = \begin{bmatrix} k_{pEdc} & 0 \\ 0 & 1 \end{bmatrix} \quad \mathbf{D}_{Edc2} = \begin{bmatrix} k_{pEdc} \\ 0 \end{bmatrix}$$

Equation (6) combined with (8) leads to the SS model of a converter with its direct-voltage controller, as follows:

$$\Delta \dot{\mathbf{x}} = \mathbf{A}_e \Delta \mathbf{x} + [\mathbf{B}_{e1} \quad \mathbf{B}_{e2}] \begin{bmatrix} \Delta \mathbf{r}_{edq}^T \\ \Delta E_{DC} \end{bmatrix} \quad (9a)$$

$$\Delta i_{DC} = \mathbf{C}_e \Delta \mathbf{x} + [\mathbf{D}_{e1} \quad \mathbf{D}_{e2}] \begin{bmatrix} \Delta \mathbf{r}_{edq}^T \\ \Delta E_{DC} \end{bmatrix} \quad (9b)$$

where:

$$\Delta \mathbf{x}^T = [\Delta i_{sdq}^T \quad \mathbf{m}_{dq}^T \quad n] \quad \Delta \mathbf{r}_{edq}^T = [\Delta r_{Edc} \quad \Delta r_q]$$

$$\mathbf{A}_e = \begin{bmatrix} \mathbf{A}_c & \mathbf{B}_{c1} \mathbf{C}_{Edc} \\ \mathbf{0} & \mathbf{0} \end{bmatrix} \quad \mathbf{B}_{e1} = \begin{bmatrix} \mathbf{B}_{c1} \mathbf{D}_{Edc1} \\ \mathbf{B}_{Edc1} \end{bmatrix} \quad \mathbf{B}_{e2} = \begin{bmatrix} -\mathbf{B}_{c1} \mathbf{D}_{Edc2} \\ -\mathbf{B}_{Edc2} \end{bmatrix}$$

$$\mathbf{C}_e = [\mathbf{C}_c \quad \mathbf{D}_{c1} \mathbf{C}_{Edc}] \quad \mathbf{D}_{e1} = \mathbf{D}_{c1} \mathbf{D}_{Edc1} \quad \mathbf{D}_{e2} = \mathbf{D}_{c2} - \mathbf{D}_{c1} \mathbf{D}_{Edc2}$$

## C. DC Grid

The SS model of a three-terminal dc grid is to be developed in this section. The dc grid is composed of cables modeled as  $\Pi$  equivalents as shown in Figure 4. The capacitors shown in Figure 4 represent an equivalent capacitor of the cable capacitor together with the converter capacitor.

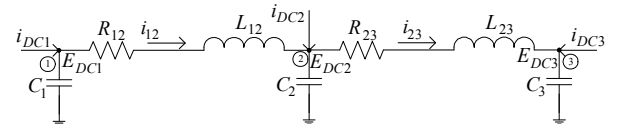


Figure 4. Three-terminal dc grid model

From Figure 4, the dc grid dynamics can be described by the following set of equations:

$$\mathbf{C}\Delta\dot{\mathbf{E}}_{DC} = -\mathbf{T}^T\Delta\dot{\mathbf{i}}_L + \mathbf{I}_{3\times 3}\Delta\dot{\mathbf{i}}_{DC} \quad (10a)$$

$$\mathbf{L}\Delta\dot{\mathbf{i}}_L = -\mathbf{R}\Delta\mathbf{i}_L + \mathbf{T}\Delta\mathbf{E}_{DC} \quad (10b)$$

where:

$$\mathbf{C} = \begin{bmatrix} C_1 & 0 & 0 \\ 0 & C_2 & 0 \\ 0 & 0 & C_3 \end{bmatrix} \quad \Delta\mathbf{E}_{DC} = \begin{bmatrix} \Delta E_{DC1} \\ \Delta E_{DC2} \\ \Delta E_{DC3} \end{bmatrix} \quad \Delta\mathbf{i}_L = \begin{bmatrix} \Delta i_{12} \\ \Delta i_{23} \end{bmatrix}$$

$$\Delta\mathbf{i}_{DC} = \begin{bmatrix} \Delta i_{DC1} \\ \Delta i_{DC2} \\ \Delta i_{DC3} \end{bmatrix} \quad \mathbf{L} = \begin{bmatrix} L_{12} & 0 \\ 0 & L_{23} \end{bmatrix} \quad \mathbf{R} = \begin{bmatrix} R_{12} & 0 \\ 0 & R_{23} \end{bmatrix} \quad \mathbf{T} = \begin{bmatrix} 1 & -1 & 0 \\ 0 & 1 & -1 \end{bmatrix}$$

The value of the elements of the  $\mathbf{T}$  matrix depends on the buses to which the inductive branch of the  $\Pi$  cable model is connected. The element is 1 if the column position corresponds to the ‘‘from bus’’ number. Similarly, the element is  $-1$  if the column position corresponds to the ‘‘to bus’’. Otherwise, zero. For example, the current  $\Delta i_{12}$  goes from bus 1 to bus 2, then the value of the element  $T_{11}$  would be 1 and the element  $T_{12}$  would be  $-1$ . The element  $T_{13}$  is zero. This procedure was also used in [13] and can be further used to develop larger dc grid models.

The SS model of the dc grid is:

$$\Delta\dot{\mathbf{x}}_g = \mathbf{A}_g\Delta\mathbf{x}_g + \mathbf{B}_g\Delta\mathbf{i}_{DC} \quad (11a)$$

$$\Delta\mathbf{E}_{DC} = \mathbf{C}_g\Delta\mathbf{x}_g \quad (11b)$$

where:

$$\Delta\mathbf{x}_g^T = [\Delta E_{DC1} \quad \Delta E_{DC2} \quad \Delta E_{DC3} \quad \Delta i_{12} \quad \Delta i_{23}]$$

$$\Delta\mathbf{E}_{DC}^T = [\Delta E_{DC1} \quad \Delta E_{DC2} \quad \Delta E_{DC3}]$$

$$\mathbf{A}_g = \begin{bmatrix} 0 & -\mathbf{C}^{-1}\mathbf{T}^T \\ \mathbf{L}^{-1}\mathbf{T} & \mathbf{L}^{-1}\mathbf{R} \end{bmatrix} \quad \mathbf{B}_g = \begin{bmatrix} \mathbf{C}^{-1} \\ \mathbf{0}_{2\times 3} \end{bmatrix} \quad \mathbf{C}_g = [\mathbf{I}_{3\times 3} \quad \mathbf{0}_{3\times 2}]$$

#### D. Complete State Space Model of the VSC-MTDC

Figure 5 shows the three-terminal system which is going to be modeled as an example. VSC<sub>1</sub> and VSC<sub>3</sub> are set to control the active power, while VSC<sub>2</sub> the direct-voltage.

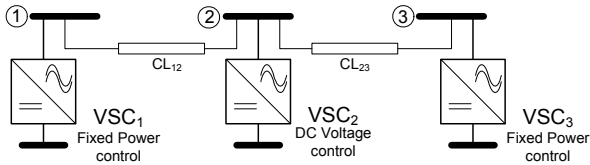


Figure 5. Three-terminal VSC-HVDC system.

The set of converters can be modeled as a single SS model as follows:

$$\Delta\dot{\mathbf{x}}_{conv} = \mathbf{A}_{conv}\Delta\mathbf{x}_{conv} + \mathbf{B}_{conv1}\Delta\mathbf{r}_{conv} + \mathbf{B}_{conv2}\Delta\mathbf{E}_{DC} \quad (12a)$$

$$\Delta\mathbf{i}_{DC} = \mathbf{C}_{conv}\Delta\mathbf{x}_{conv} + \mathbf{D}_{conv1}\Delta\mathbf{r}_{conv} + \mathbf{D}_{conv2}\Delta\mathbf{E}_{DC} \quad (12b)$$

where:

$$\Delta\mathbf{x}_{conv}^T = [\Delta\mathbf{x}_1^T \quad \Delta\mathbf{x}_2^T \quad \Delta\mathbf{x}_3^T] \quad \Delta\mathbf{r}_{conv}^T = [\Delta\mathbf{r}_{dq1}^T \quad \Delta\mathbf{r}_{edq2}^T \quad \Delta\mathbf{r}_{dq3}^T]$$

$$\Delta\mathbf{i}_{DC}^T = [\Delta i_{DC1} \quad \Delta i_{DC2} \quad \Delta i_{DC3}] \quad \Delta\mathbf{E}_{DC}^T = [\Delta E_{DC1} \quad \Delta E_{DC2} \quad \Delta E_{DC3}]$$

$$\mathbf{A}_{conv} = \begin{bmatrix} \mathbf{A}_{c1} & \mathbf{0} & \mathbf{0} \\ \mathbf{0} & \mathbf{A}_{e2} & \mathbf{0} \\ \mathbf{0} & \mathbf{0} & \mathbf{A}_{c3} \end{bmatrix} \quad \mathbf{B}_{conv1} = \begin{bmatrix} \mathbf{B}_{c1-1} & \mathbf{0} & \mathbf{0} \\ \mathbf{0} & \mathbf{B}_{e1-2} & \mathbf{0} \\ \mathbf{0} & \mathbf{0} & \mathbf{B}_{c1-3} \end{bmatrix}$$

$$\mathbf{B}_{conv2} = \begin{bmatrix} \mathbf{B}_{c2-1} & \mathbf{0} & \mathbf{0} \\ \mathbf{0} & \mathbf{B}_{e2-2} & \mathbf{0} \\ \mathbf{0} & \mathbf{0} & \mathbf{B}_{c2-3} \end{bmatrix} \quad \mathbf{C}_{conv} = \begin{bmatrix} \mathbf{C}_{c1} & \mathbf{0} & \mathbf{0} \\ \mathbf{0} & \mathbf{C}_{e2} & \mathbf{0} \\ \mathbf{0} & \mathbf{0} & \mathbf{C}_{c3} \end{bmatrix}$$

$$\mathbf{D}_{conv1} = \begin{bmatrix} \mathbf{D}_{c11} & \mathbf{0} & \mathbf{0} \\ \mathbf{0} & \mathbf{D}_{e12} & \mathbf{0} \\ \mathbf{0} & \mathbf{0} & \mathbf{D}_{c13} \end{bmatrix} \quad \mathbf{D}_{conv2} = \begin{bmatrix} \mathbf{D}_{c21} & \mathbf{0} & \mathbf{0} \\ \mathbf{0} & \mathbf{D}_{e22} & \mathbf{0} \\ \mathbf{0} & \mathbf{0} & \mathbf{D}_{c23} \end{bmatrix}$$

The matrices  $\mathbf{A}_{c1}$ ,  $\mathbf{A}_{e2}$ ,  $\mathbf{A}_{c3}$ ,  $\mathbf{B}_{c1}$ ,  $\mathbf{B}_{e2}$ ,  $\mathbf{B}_{c3}$ , etc. are the individual matrices obtained for every converter using the procedure indicated in the previous section.

Now, (11) and (12) can be combined to obtain the SS model of the VSC-MTDC system.

$$\Delta\dot{\mathbf{x}}_{sys} = \mathbf{A}_{sys}\Delta\mathbf{x}_{sys} + \mathbf{B}_{sys}\Delta\mathbf{r}_{sys} \quad (13a)$$

$$\Delta\mathbf{y}_{sys} = \mathbf{C}_{sys}\Delta\mathbf{x}_{sys} \quad (13b)$$

where:

$$\Delta\mathbf{x}_{sys}^T = [\Delta\mathbf{x}_{conv}^T \quad \Delta\mathbf{x}_g^T] \quad \Delta\mathbf{r}_{sys}^T = \Delta\mathbf{r}_{conv}^T$$

$$\mathbf{A}_{sys} = \begin{bmatrix} \mathbf{A}_{conv} & \mathbf{B}_{conv2}\mathbf{C}_g \\ \mathbf{B}_g\mathbf{C}_{conv} & \mathbf{A}_g + \mathbf{B}_g\mathbf{D}_{conv2}\mathbf{C}_g \end{bmatrix} \quad \mathbf{B}_{sys} = \begin{bmatrix} \mathbf{B}_{conv1} \\ \mathbf{B}_g\mathbf{D}_{conv1} \end{bmatrix}$$

$\mathbf{C}_{sys}$  can be selected in such a way that some desired states are obtained as outputs. From the SS model (13) the dynamic characteristics of the VSC-MTDC system can be obtained by calculating the eigenvalues.

Finally, as can be seen in (2), there are matrix elements which depend on the chosen operating conditions. The initial values of the dc grid ( $E_{DC0}$ ,  $P_{DC0}$ ) are calculated iteratively with a Newton-Raphson algorithm, while the initial values of the ac side ( $V_{cd0}$ ,  $V_{cq0}$ ,  $i_{sd0}$ ,  $i_{sq0}$ ) are calculated algebraically.

### III. EIGENVALUE ANALYSIS

The analysis is performed by calculating the eigenvalues of the system for different operating points. First, two two-terminal systems are evaluated due to their simplicity. A more detailed model is also developed in PSCAD in order to compare the findings of the analysis. Afterwards, a three-terminal system is also tested. The controller parameters are often selected assuming ideal conditions. However, it is shown in the analysis that the dc grid dynamics can influence, as well, the overall performance of the system. The criteria to select the converter elements are presented next.

#### A. Model Data and Parameters

##### 1) Converter

The converters are considered identical having the rating data of 600 MVA and  $\pm 300$  kV. A series reactance of 0.25 pu is considered to represent the phase reactor in series with transformer reactance. A resistance equal to 1 % of the total reactance is considered. The value of the converter capacitor is calculated using 5 ms charging time, as proposed in [14].

##### 2) Current controller

The proportional and the integral gains of the current controller are usually selected in such a way that the closed

loop system becomes a first order system with bandwidth of  $\alpha$ . In order to achieve that, the gains are selected as [15]:

$$k_{pcc} = \alpha L \quad k_{icc} = \alpha R \quad (14)$$

Here  $\alpha$  is selected as 4 pu (50 Hz frequency base), as recommended in [16].

### 3) Direct-voltage controller

In [11] and [17] similar formulas were derived in order to find the proper values for the proportional and the integral gains of the direct-voltage controller. In the work presented here the following formulas are adopted from [17]:

$$k_{pEdc} = \alpha_{Edc} \xi C, \quad k_{iEdc} = \frac{\alpha_{Edc}^2 C}{2} \quad (15)$$

where  $\alpha_{Edc}$  is the undamped resonance frequency and  $\xi$  is the damping ratio. It is shown in [17] that the  $\xi$  plays a major role in damping oscillations. In this paper,  $\alpha_{Edc}$  is set to both, 0.4 (10 % of  $\alpha$  as recommended in [17]) and 0.8, and  $\xi$  is set to 3 (as recommended in [17]). Note that those gains are calculated under the assumption that the VSC is connected to only its capacitor and not to a cable, as in this case.

### 4) Cable

The cable parameters correspond to one with ratings of 600 MW and  $\pm 300$  kV. The conductor cross section area is about 2000 mm<sup>2</sup> (1000 A ampacity) and the resistivity is 3.9e-8  $\Omega$ -m. The insulation thickness is 24 mm, and the relative permittivity is 2.5. The parameters used for calculation of a  $\Pi$  model (at the fundamental frequency) are shown in Table I.

TABLE I. CABLE DATA

Resistance ( $\Omega$ /km)	Inductance (mH/km)	Capacitance ( $\mu$ F/km)
0.0376	0.189	0.207

## B. Study Cases

### 1) Two terminal system

Two configurations of two-terminal systems are analysed. One in which VSC<sub>1</sub> and VSC<sub>2</sub> are connected in a back-to-back configuration; and another configuration in which VSC<sub>1</sub> and VSC<sub>2</sub> are interconnected through a 50km cable whose characteristics are described in Table I. In both cases VSC<sub>1</sub> controls the direct-voltage, while VSC<sub>2</sub> controls the power. The controller parameters are set as recommended in the previous section. Figure 6 shows the location of the eigenvalues as the power set-point of VSC<sub>2</sub> changes from +1 pu to -1 pu (positive means power from the ac side to the dc side, negative means the opposite) for the two configurations. In addition, for each configuration two cases are calculated, with  $\alpha_{Edc}$  set as 0.4 and  $\alpha_{Edc}$  is set as 0.8.

For the back-to-back case, it can be seen that for both values of  $\alpha_{Edc}$  the eigenvalues remain inside the well damped area in most of the cases. When  $\alpha_{Edc}$  is set as 0.8 the eigenvalues start moving outside the well damped area, but they still remain inside the stable region. The most critical case is when the power at VSC<sub>1</sub> is +1 pu.

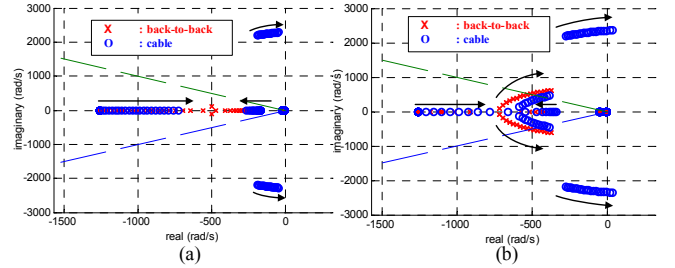


Figure 6. Pole placement as the power changes from +1 pu to -1 pu (with steps of -0.1) at VSC<sub>2</sub>. (a)  $\alpha_{Edc}$  is set as 0.4. (b)  $\alpha_{Edc}$  is set as 0.8.

For the second configuration, as it can be seen in Figure 6, new eigenvalues appear as a result of the dynamics of the cable connecting VSC<sub>1</sub> and VSC<sub>2</sub> and it can be seen that they approach the imaginary axis as the power grows to +1 pu at VSC<sub>1</sub> being the most critical case when the power is +1 pu. When  $\alpha_{Edc}$  is set as 0.8, some eigenvalues even go into right half plane for powers greater than 0.8 pu at VSC<sub>1</sub>.

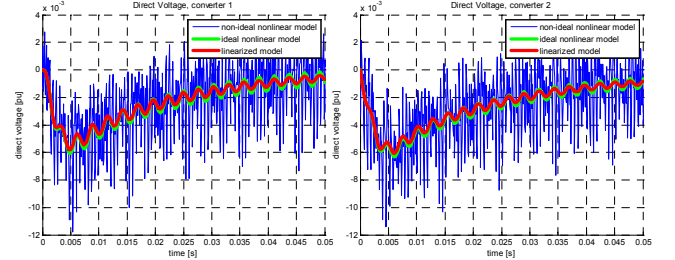


Figure 7. Direct-voltage at each VSC's dc node for a power step from -0.7 to -0.75 at VSC<sub>2</sub>. (a) Direct-voltage at VSC<sub>1</sub>. (b) Direct-voltage at VSC<sub>2</sub>.

The comparison between the results of state space model and with the results of two different PSCAD models is shown in Figure 7. In one of the PSCAD model the switches are modelled in detail (non-ideal nonlinear model), therefore, the curves present a high harmonic content. In the other PSCAD model, the VSC is represented as an ideally controlled voltage source in the ac side, and an ideally controlled current source in the dc side (ideal nonlinear model). The direct-voltages at both VSC's dc nodes are plotted as a result of a step change in the power at VSC<sub>2</sub> from -0.70 pu to -0.75 pu. It can be seen that the linearized model and the ideal PSCAD model oscillate with the same frequency, although the linearized model is more damped. This is due to the fact that, in the PSCAD model, the increase of power makes the eigenvalues to move closer imaginary axis, meaning that the damping of the system decreases. The detailed PSCAD model shows a similar pattern although the oscillations are not observed since the high frequency harmonics override them. The comparison shows good agreement between the linearized state space model and both models in PSCAD.

### 2) Three-terminal system

The calculations of the eigenvalues are performed for a three-terminal system as the one in Figure 4, where the length of the cables CL<sub>12</sub> and CL<sub>23</sub> are each 50 km. The controller parameters are set with the criteria indicated in Section III.A. In this case, the power set-points of the VSC<sub>1</sub> and VSC<sub>3</sub> are changed from 0.5 to -0.5 simultaneously making the power through VSC<sub>2</sub> to change from -1 to +1 pu. As in the two-

terminal cases, two values of  $\alpha_{Edc}$  are tested:  $\alpha_{Edc}$  set as 0.4 and  $\alpha_{Edc}$  set as 0.8.

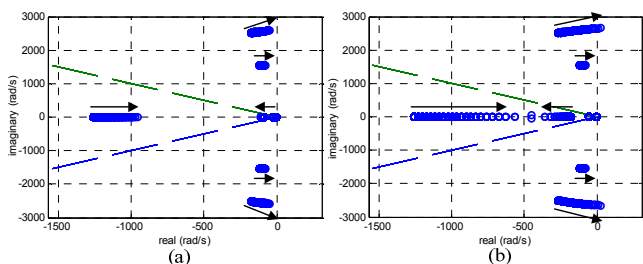


Figure 8. Pole placement as the power changes from +1 pu to -1 pu (with steps of -0.1) at VSC<sub>2</sub>. (a)  $\alpha_{Edc}$  is set as 0.4. (b)  $\alpha_{Edc}$  is set as 0.8.

Similarly to the two-terminal cases, the increase of power at VSC<sub>2</sub> towards 1.0 pu deteriorates the dynamical performance of the system. It is also verified that, with  $\alpha_{Edc}$  set to 0.8 pu, some eigenvalues move to the right half plane when the power at VSC<sub>2</sub> is greater than 0.8 pu. This case is investigated in the PSCAD models where power at VSC<sub>2</sub> is ramped up from +0.7 pu to +1.0 pu with a rate of 0.10 pu/s, for both values of  $\alpha_{Edc}$ . In Figure 9 (a) it is shown that, in the first case, the system remains stable after reaching 1 pu, while in the second case undamped oscillations appear.

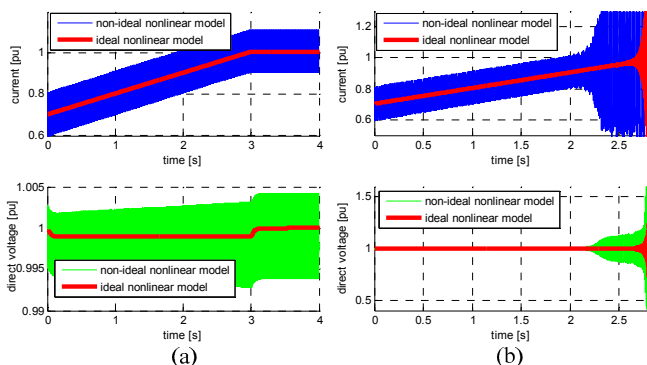


Figure 9. Direct voltage and current from VSC2 for a ramp up of power at VSC<sub>1</sub> and VSC<sub>3</sub> (a)  $\alpha_{Edc}$  is set as 0.4. (b)  $\alpha_{Edc}$  is set as 0.8.

#### IV. CONCLUSIONS

In this paper, a procedure to develop a state space model for VSC-MTDC systems was presented. Since the system is nonlinear, it is linearized assuming small signal perturbations around an operating point. The state space model allows the calculation of the eigenvalues of the system for different loading conditions. Assumptions were made in order to simplify the complexity of the system and to make the ac side of the VSC not to impact the dc system.

The analysis carried out in this paper was made using recommended parameters [11], [14]-[17]. In particular, the recommended direct-voltage controller gains were obtained under the consideration that the VSC is connected only to its capacitor [11], [17]. It has been shown that, for a back to back configuration, those gains produce a good dynamical performance for all the tested operating points. However, when the dynamics of the cables are considered, the performance deteriorates, appearing oscillations which

become poorly damped as the power increases at the VSC which controls the direct-voltage. That means that, in order to select the gains such that the system shows a good performance for all operating point, the dc grid dynamics should be taken into account. More detailed representation of the dc grid may result in new dynamics, which must be further investigated.

#### REFERENCES

- [1] EWEA, "Oceans of Opportunity," September 2009, available from: [http://www.ewea.org/fileadmin/ewea\\_documents/documents/publications/reports/Offshore\\_Report\\_2009.pdf](http://www.ewea.org/fileadmin/ewea_documents/documents/publications/reports/Offshore_Report_2009.pdf)
- [2] B. Jacobson, P. Karlsson, G. Apslund, L. Harnefors, T. Jonsson, "VSC-HVDC Transmission with Cascaded Two-Level Converters", Cigrè session 2010, Paris, 22-27 August 2010.
- [3] G. Pinares, M. Bollen, "Understanding the Operation of HVDC Grids," Cigrè International Symposium: The Electric Power System of the Future, Integrating supergrids and microgrids, Bologna, Italy, 13-15 September 2011.
- [4] T. M. Hailesalassie, M. Molinas, T. Undeland, "Multi-terminal VSC-HVDC System for Integration of Offshore Wind Farms and Green Electrification of Platforms in the North Sea," NORPIE 2008, Espoo, Finland, 9 - 11 June, 2008.
- [5] T. M. Hailesalassie, K. Uhlen, T. Undeland, "Control of Multiterminal HVDC Transmission for Offshore Wind Energy," Nordic Wind Power Conference, Bornholm, Denmark, 10 - 11 September 2009.
- [6] C. D. Barker, R. Whitehouse, "Autonomous Converter Control in a Multi-terminal HVDC System," 9<sup>th</sup> International Conference on AC and DC Power Transmission, London, UK, 19-21 October, 2010.
- [7] A.M. Alseid, D. Jovicic, A. Starkey, "Small signal modelling and stability analysis of multiterminal VSC-HVDC," *Power Electronics and Applications (EPE 2011), Proceedings of the 2011-14th European Conference on*, vol., no., pp.1-10, Aug. 30 2011-Sept. 1 2011.
- [8] E. Prieto-Araujo, F. D. Bianchi, A. Junyent-Ferré, O. Gomis-Bellmunt, "Methodology for Droop Control Dynamic Analysis of Multiterminal VSC-HVDC Grids for Offshore Wind Farms," *IEEE Trans. on Power Delivery*, vol.26, no.4, pp.2476-2485, Oct. 2011
- [9] G.O. Kalcon, G. P. Adam, O. Anaya-Lara, S. Lo, K. Uhlen, "Small-Signal Stability Analysis of Multi-terminal VSC-Based DC Transmission Systems," *IEEE Trans. On Power Systems*, vol.27, no.4, pp.1818-1830, Nov. 2012.
- [10] S. Cole, "Steady State and Dynamic Modelling of VSC HVDC Systems for Power System Simulations," PhD Thesis, Katholieke Universiteit Leuven, Leuven, Belgium, 2010.
- [11] L. Zhang, "Modeling and Control of VSC-HVDC Links Connected to Weak AC System," PhD Thesis, Royal Institute of Technology, Stockholm, Sweden, 2010.
- [12] L. Tang, "Control and Protection of Multi-Terminal DC Transmission Systems Based on Voltage-Source Converters," PhD Thesis, pp.42-62, McGill University, Montreal, Quebec, Canada, 2003.
- [13] S. M. Fragoso Rodrigues, "Dynamic Modeling and Control of VSC-based Multi-terminal DC Networks," Master thesis, Universidade Técnica de Lisboa, December, 2011.
- [14] It is time to connect - Technical description of HVDC light® technology. Available from <http://www.abb.com/hvdc>, 2009-06-25.
- [15] L. Harnefors, "Model-Based Current Control of AC Machines Using the Internal Model Control Method," *IEEE Trans. On Industry Applications*, vol. 34, no.1, pp.133-141, Jan/Feb, 1998.
- [16] L. Harnefors, M. Bongiorno, S. Lundberg, "Input-Admittance Calculation and Shaping for Controlled Voltage-Source Converters," *IEEE Trans. On Industrial Electronics*, vol 54, no.6, pp.3323-3334, Dec. 2007.
- [17] G. Pinares, "Operation of HVDC grids in parallel with AC grids," Master of Science Thesis, Chalmers University of Technology, Sweden, 2010.